Icosahedral crystals: neutron diffraction tells you where the atoms are

1989 J. Phys.: Condens. Matter 1 1029

(http://iopscience.iop.org/0953-8984/1/6/001)

J. Phys.: Condens. Matter **1** (1989) 1029–1048. Printed in the UK

Icosahedral crystals: neutron diffraction tells you where the atoms are

C Janot†, M De Boissieu†‡, J M Dubois‡ and J Pannetier†
† Institut Laue–Langevin, 156X, 38042 Grenoble Cédex, France
‡ LSG2M, Ecole des Mines, Parc de Saurupt, 54042 Nancy Cédex, France

Received 10 May 1988, in final form 22 August 1988

Abstract. Neutron diffraction data were obtained from a single-phase icosahedral powder of the system $Al_{74}Si_5Mn_{21}$ and its modification by isomorphous substitution on the Mn sites. Amplitudes and phase differences of the partial structure factors (F_{Al}, F_{Mn}) were determined. From their $Q_\perp$-dependences within a strip-projection approach, phases were reconstructed. Atomic densities were then calculated in the physical space and in the six-dimensional periodic lattice, resulting in the first experimentally deduced decoration of the quasi-periodic network. The Mackay icosahedron no longer appears as the necessary basic structural unit. In six dimensions the structure has a simple CsCl-like space-group symmetry.

1. Introduction

Quasi-periodic structures have been shown to be derivable from what is now called the strip-projection method (SPM) [1–7]. They are also conceptually equivalent to three-dimensional Penrose tiling (3DPT) [8], which is a structure known for more than a decade to exhibit five-fold symmetries and Bragg peak diffraction. The second stage necessary in order to specify the structure of a quasi-crystal is the 'decoration' of the geometrical framework. The decoration is the rule for placing atoms within the rigid geometry. Different models have been proposed to decorate a 3DPT [9–11], but to date there has been no atomic decoration scheme directly deduced from diffraction data, beyond the determination of partial pair distribution functions [12].

This is indeed intrinsically more difficult for a quasi-crystal than for a crystal. A perfect quasi-periodic structure, without any disorder, still has an infinite number of sites which are not exactly equivalent. One should have expected that the whole apparatus of crystallography and diffraction patterns could be applicable, in 6D space, to the 6D periodic crystal from which the 3D quasi-crystal is generated using the SPM. Unfortunately there are some conceptual and/or practical difficulties to be overcome related to the fairly low level of information that can be extracted from the classical diffraction patterns of quasi-crystals: a very small number of the diffracted features can really be measured and each of them contains mixed contributions from the structure factor of the 6D Bravais lattice, the chemical decoration of the projected structure in 3D and the Fourier transform of the strip cut in 6D.

A step towards the separation of these different contributions to the diffracted intensity was made by using contrast variation in neutron diffraction experiments [13–

0953-8984/89/061029 + 20 $02.50

16], which allowed one to determine amplitudes and phase differences of the partial structure factors F_{Al} and F_{Mn} in Al–Mn icosahedral phases.

The present work intends to proceed further in achieving this separation and reports on a phase reconstruction procedure for F_{Al} and F_{Mn}, along with calculations of the partial atomic densities.

2. Experiment and data analysis

The use of neutrons is particularly attractive in studying the atomic structure of Al–Mn compounds, because the neutron scattering length of Mn is negative ($b_{Mn} = -0.373 \times 10^{-12}$ cm) and because Mn atoms are expected to be substituted by Cr or Fe, which are positive neutron scatterers ($b_{Cr} = +0.364 \times 10^{-12}$ cm; $b_{Fe} = +0.954 \times 10^{-12}$ cm), without too much disturbance of the structure [17]. In fact, it has been shown [18] that the substitution of Cr or Fe for Mn is not perfectly isomorphous in icosahedral phases. In other words, even if the phases containing Cr or Fe remain apparently icosahedral according to electron diffraction criteria, they might have atomic decorations different from that of Al–(pure Mn) compounds. Fortunately enough, the substitution of an equi-atomic FeCr mixture (the so-called σ-phase) for Mn happened to be isomorphous and random [12, 14, 15].

Let the composition of the investigated quasi-crystalline phase be described by the formula $Al_x(Mn_{1-c}\sigma_c)_{1-x}$ in which σ stands for the equi-atomic FeCr substitute. The average coherent scattering length b_T of the $Mn_{1-c}\sigma_c$ mixture is given by

$$b_T = (1 - c)b_{Mn} + cb_\sigma$$

(with $b_{Mn} = -0.373 \times 10^{-12}$ cm and $b_\sigma = +0.658 \times 10^{-12}$ cm). Thus a modulation of the total structure factor $F_c(Q)$ is obtained as a function of the substitution rate c, for each measured value of the scattering vector Q. Then, the contributions from the aluminium and transition-metal atoms to the diffracted intensities can be separated and the partial structure factor calculated [14, 19].

Quasi-crystalline phases of the Al–Mn system can be produced by melt spinning as described in detail elsewhere [13, 20]. The icosahedral phase (IP) currently forms in alloys with Mn concentration ranging from 14 to 22%, in coexistence with a residual FCC Al phase whose volume fraction is minimised for a nominal composition of the quenched alloys corresponding to $Al_{80}Mn_{20}$. Despite the stoichiometry of the IP being apparently in the vicinity of Al_4Mn, it is far from easy to produce samples of pure IP at or near this ideal composition. The decagonal phase (DP) then forms in competition with the IP and can even be obtained alone by reducing the solidification rate slightly [21]. However, the formation of the IP in Al–Mn alloys has been shown to be favoured by the addition of silicon, and pure IP can even be produced if the silicon content reaches about 5 at. % [19]. Consequently, the neutron diffraction data analysed in this paper were measured with five samples of the system $Al_{74}Si_5(Mn_{1-c}\sigma_c)_{21}$ (nominal composition) with $c = 0, 0.140, 0.362, 0.696$ and 1, corresponding to $b_T = -0.373, -0.228, 0, +0.3445$ ($= b_{Al}$) and $+0.658$ (in 10^{-12} cm), respectively. According to their electron diffraction patterns and electron micrographs the quenched alloys appeared as single icosahedral phases except for $Al_{74}Si_5Mn_{21}$ ($c = 0$) in which the presence of about 3% of the hexagonal β-phase cannot be avoided. For the purpose of neutron diffraction measurements, these samples were finely powdered and packed into a cylindrical vanadium can (diameter 8 mm, height 50 mm). The neutron data were collected at the High Flux Reactor facilities

of the Institut Laue–Langevin (ILL, Grenoble). High-resolution powder diffraction patterns were obtained using the new D2B two-axis diffractometer. Its bank of 64 counters, at intervals of 2.5°, covers an angular range $2\theta = 160°$ and can be moved by steps of 0.020°. This instrument is intended to be a very-high-resolution, high-intensity powder diffractometer equipped with 5′ Söller collimators both in the primary beam and in front of the 64 detectors [22]. Diffraction peaks measured with the icosahedral phase do not require the full resolution of the machine and these materials are rather poor scatterers. Thus, the incident Söller collimators were removed, reducing the resolution to about $\Delta Q/Q = 5 \times 10^{-3}$ but with a gain of a factor of about 7 in neutron flux. The wavelength of the monochromatised neutron beam ($\lambda = 1.5947$ Å) and the angular distances between elements of the detector bank were calibrated with an yttrium iron garnet (YIG) and an NBS Al_2O_3 standard. Each measured diffraction pattern was accumulated over a period of about 15 h. The five diffraction patterns measured at room temperature, in a Q-range of 8 Å^{-1}, are shown in figure 1. The patterns were analysed, as fully explained elsewhere [13–15], using the maximum-likelihood fitting procedure usually applied to Poisson diffraction spectra [23] to obtain intensities, positions and widths of the peaks, with standard deviations on these quantities. The absence of significant shifts in peak positions due to the chemical substitutions of σ-FeCr for Mn was checked carefully. These positions, reconverted into scattering vectors $Q = (4\pi/\lambda) \sin\theta$, were then indexed according to

$$Q = \frac{2\pi}{a}\left(\frac{N + \tau M}{2(2 + \tau)}\right)^{1/2} \tag{1}$$

which is expected if the structure is assumed to exhibit icosahedral symmetries [24]. In equation (1) N takes any even value and M is an integer which conforms to the limits $-N/\tau < M < N/\tau$ [24]; $\tau = 2\cos 36° = (1 + \sqrt{5})/2 = 1.618034\ldots$ is the golden mean. The best fit of equation (1) to data led to $a = 6.497$ Å within a relative accuracy better than 3×10^{-3} for the 60 diffraction peaks measured with each sample. It has been shown [24] that such a sequence of positions is equivalent to a six-integer indexing $h/h'\ k/k'\ l/l'$ related to a primitive cubic lattice in six dimensions with a as the lattice parameter. These six indices are related to N and M according to

$$\begin{aligned} N &= h^2 + h'^2 + k^2 + k'^2 + l^2 + l'^2 \\ M &= h'^2 + k'^2 + l'^2 + 2(hh' + kk' + ll') \end{aligned} \tag{2}$$

and must conform to well defined parity and scaling properties [24]. The six-index notation, however, is merely a shorthand for indexing irrational numbers of the form $h + h'\tau$. The use of a cubic basis [24] to represent wavevectors, instead of an icosahedral one, allows one to develop most of the geometry without recourse to six dimensions but, of course, hides the icosahedral symmetry somewhat.

Intensities of the diffraction peaks were carefully corrected for absorption, Lorentz factor and Debye–Waller thermal effects (a Debye temperature equal to 380 K was determined from the temperature dependence of some of the strongest diffraction peaks). Peak positional powder data can be reconverted into 3D diffraction $\boldsymbol{Q}$-vectors by distributing the total integrated intensities over the corresponding set of equivalent reflections [14, 15] (indexing and multiplicity being accounted for). The $I(\boldsymbol{Q})$ intensities may be written as

$$I(\boldsymbol{Q}) = |b_{Al}F_{Al} + b_T F_T|^2 \tag{3}$$

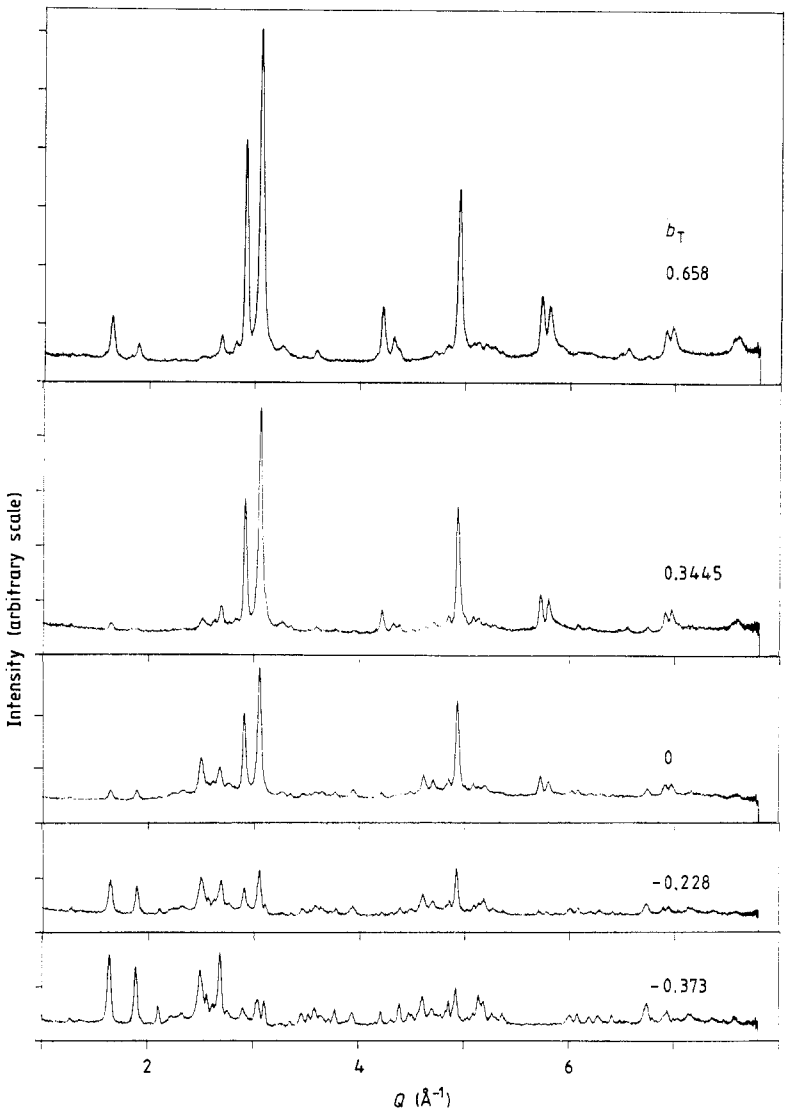

Figure 1. High-resolution neutron diffraction patterns of the icosahedral phase $Al_{74}Si_5TM_{21}$ with changing contrast b_T on the TM sites. The positive value $b_T = +0.658 \times 10^{-12}$ cm reproduces the contrast between Al and Mn when observed with x-rays. Comparing patterns $b_T = 0$ and $b_T = +0.658 \times 10^{-12}$ cm shows that x-ray patterns are mainly influenced by Al scattering. For phase-shift reasons, the information contained in the diffraction patterns happens to be the greatest for the largest negative value of the scattering length on the transition-metal sites. Quite a large amount of 'diffuse scattering' also shows up, especially below the Bragg diffraction for the pattern $b_T = 0$, which measures scattering from the aluminium subnetwork alone.

where the b stand for the neutron scattering lengths of aluminium and average transition-metal atoms respectively, and the F are the partial structure factors defined by

$$F_{Al} = \sum_{Al} \exp(i\boldsymbol{Q} \cdot \boldsymbol{r}_{Al}) \qquad F_T = \sum_{T} \exp(i\boldsymbol{Q} \cdot \boldsymbol{r}_T). \tag{4}$$

An equivalent expression for $I(\boldsymbol{Q})$ is then

$$I(\boldsymbol{Q}) = b_{\mathrm{Al}}^2|F_{\mathrm{Al}}|^2 + b_{\mathrm{T}}^2|F_{\mathrm{T}}|^2 + 2b_{\mathrm{Al}}b_{\mathrm{T}}|F_{\mathrm{Al}}||F_{\mathrm{T}}|\cos(\Delta\varphi) \tag{5}$$

in which $\Delta\varphi$ is the phase difference between F_{Al} and F_{T}. Obviously, equation (5) contains $|F_{\mathrm{Al}}|$, $|F_{\mathrm{T}}|$ and $|\Delta\varphi|$ as three unknown quantities, which can be determined, for each $\boldsymbol{Q}$ reflection, by measuring at least three independent intensities $I(\boldsymbol{Q}, b_{\mathrm{T}})$ with three samples that are strictly identical except for their neutron scattering contrast b_{T} on the transition-metal (TM) sites. Actually, more than three contrast values are required due to the necessary rescaling procedure of the diffraction patterns with respect to each other [14, 25]. Equations (3) to (5) obviously are only valid for true binary Al–TM alloys, or pseudo-binary alloys, in which TM is a random mixture of transition metals (isomorphous substitution). The question remains of what to do with the 5 at.% Si included in the icosahedral phases. In the present work, it has been chosen, somewhat arbitrarily, to treat Al and Si atoms as a single (average) atomic species. Such an assumption is equivalent to considering that Al and Si atoms are randomly distributed on the sites of one subnetwork with an average scattering length

$$\langle b\rangle_{\mathrm{Al,Si}} = c_{\mathrm{Al}}b_{\mathrm{Al}} + c_{\mathrm{Si}}b_{\mathrm{Si}} = 0.3493 \quad (\text{in } 10^{-12}\,\text{cm})$$

only 1% larger than b_{Al}. If, on the contrary, a maximum chemical order were assumed, such that Si atoms would have only Si–Al bonds, the intensity diffracted by Al and Si atoms altogether would be proportional to

$$c_{\mathrm{Al}}^2 b_{\mathrm{Al}}^2 + 2c_{\mathrm{Al}}c_{\mathrm{Si}}b_{\mathrm{Al}}b_{\mathrm{Si}} = 0.07573$$

which is equivalent to an average scattering length of 0.3483. Obviously, the two cases, and any other case in between, cannot be experimentally distinguished and the problem can reasonably be treated within the 'binary alloy' approximation. To go further requires a specific study of the Si positions, using for instance contrast changes produced with Ge substitution. This is far from easy and has not been carried out so far.

The raw product of the neutron diffraction data with contrast variation is then the triple set $|F_{\mathrm{Al}}(\boldsymbol{Q})|$, $|F_{\mathrm{T}}(\boldsymbol{Q})|$, $|\Delta\varphi(\boldsymbol{Q})|$. As already observed with other icosahedral alloys [14] the phase differences $\Delta\varphi$ measured in the present work happened to be all equal to 0 or π, within experimental accuracy, which suggests centrosymmetric properties of the structure. As a consequence, the measured partial structure factors F_{Al} and F_{T} of the icosahedral phase can be expressed by pairs of real numbers, either of the same or of opposite signs, multiplied by a common phase factor $\exp(\mathrm{i}\Phi)$. However, within a given pair, which of F_{Al} or F_{T} is positive or negative and their common phase $\Phi(\boldsymbol{Q})$ cannot be deduced from diffraction data and a phase reconstruction procedure must be discovered if one wishes to proceed beyond the usual Patterson function analysis [26]. This can be obtained as a consequence of 3D quasi-periodic structures having translational symmetries when described in a higher-dimensional space, owing to the fact that the icosahedral point group is compatible with translational space groups in six dimensions though rejected by any 3D space group. Such a scheme can be explained within the strip-projection approach.

In the formulation of the strip-projection method one starts with a 6D primitive cubic lattice in R_6 which is projected onto two orthogonal well chosen 3D subspaces $\mathrm{R}_{3\parallel}$ and $\mathrm{R}_{3\perp}$. The quasi-periodic crystal consists in projection onto $\mathrm{R}_{3\parallel}$ of those points of the 6D cubic lattice that are within a strip S_6 extending infinitely parallel to $\mathrm{R}_{3\parallel}$ but having a finite cross section $A_{3\perp}$ in $\mathrm{R}_{3\perp}$ called the acceptance function. In its simplest description $A_{3\perp}$ is equal to 1 inside the strip and 0 outside. The 6D diffraction pattern of the infinite

real 6D cubic lattice would be a 6D cubic distribution of Dirac functions at vectors $\boldsymbol{Q}_6$. The 6D diffraction pattern of the strip S_6 would also be a 6D distribution of extended spots centred at $\boldsymbol{Q}_6$, still Dirac-like when scanned at $\boldsymbol{Q}_\parallel$-vectors in the 3D reciprocal space associated with $R_{3\parallel}$, but broadened in the orthogonal 3D reciprocal subspace associated with $R_{3\perp}$ due to convolution with the Fourier transform $G(\boldsymbol{Q}_\perp)$ of the acceptance function $A_{3\perp}(\boldsymbol{Q}_\perp$ and $\boldsymbol{Q}_\parallel$ are the projections of $\boldsymbol{Q}_6$ into the two 3D reciprocal subspaces $R^*_{3\perp}$ and $R^*_{3\parallel}$ associated with $R_{3\perp}$ and $R_{3\parallel}$, respectively). In summary, we have the following:

(i) The density of the 6D primitive cubic lattice is taken equal to $\rho(\boldsymbol{r}_6) = \delta(\boldsymbol{r}_6)$ where $\delta(\boldsymbol{r}_6)$ stands for a set of Dirac density peaks sited at the vertices of the 6D primitive cubic lattice.

(ii) The density within the strip can then be written as $\delta(\boldsymbol{r}_6)\cdot A_{3\perp}(\boldsymbol{r}_\perp)$, with $\boldsymbol{r}_\perp$ the component of $\boldsymbol{r}_6$ in $R_{3\perp}$.

(iii) The diffraction pattern of the strip is described by the Fourier transform (FT) $\delta(\boldsymbol{Q}_6) * G(\boldsymbol{Q}_\perp)$, in which $\delta(\boldsymbol{Q}_6)$ is the set of Dirac peaks transformed from $\delta(\boldsymbol{r}_6)$ and $*$ stands for a convolution product.

(iv) The diffraction features are investigated only in the observation reciprocal space $R^*_{3\parallel}$, at each $\boldsymbol{Q}_\parallel$-value corresponding to a single given $\boldsymbol{Q}_6$ (due to irrationality of the projection). Thus the scattering vectors $|\boldsymbol{Q}| = (4\pi/\lambda)\sin\theta$ have to be identified with $\boldsymbol{Q}_\parallel$ in equations (3) to (5) and the diffracted intensities are the square of the modulus of $\delta(\boldsymbol{Q}_6)\cdot G(\boldsymbol{Q}_\perp)$.

(v) If these $\delta(\boldsymbol{Q}_\perp)\cdot G(\boldsymbol{Q}_\perp)$ diffraction-deduced structure factors are directly Fourier-transformed, one gets $\delta(\boldsymbol{r}_6) * A_{3\perp}(\boldsymbol{r}_\perp)$, that is the set of Dirac density peaks of the infinite primitive cubic lattice 'decorated' by the acceptance function $A_{3\perp}$.

(vi) Finally, the atomic density in our 3D physical space can be obtained by cutting $\delta(\boldsymbol{r}_6) * A_{3\perp}(\boldsymbol{r}_\perp)$ with $R_{3\parallel}$.

All these statements are strictly valid for a monatomic system only but contrast variations, as used in the present work, allow one to calculate the partial structure factors for Al and TM atoms separately, as will now be explained, and thus to treat the binary problem as two independent monatomic systems. In such a formulation, the partial structure factors F_{Al} and F_T actually determined in 3D can be expressed, for each Al or TM site, as

$$F_{Al}(\boldsymbol{Q}_\parallel) = \delta_{Al}(\boldsymbol{Q}_6)G_{Al}(\boldsymbol{Q}_\perp) \qquad F_T(\boldsymbol{Q}_\parallel) = \delta_T(\boldsymbol{Q}_6)G_T(\boldsymbol{Q}_\perp) \tag{6}$$

in which δ and G still stand for the structure factors of the infinite periodic structure in R_6 and the FT of the pertinent partial acceptance functions in $R_{3\perp}$ respectively. Let us first analyse the data corresponding to $F_T(\boldsymbol{Q}_\parallel) = \delta_T(\boldsymbol{Q}_6)G_T(\boldsymbol{Q}_\perp)$, i.e. the partial structure factor of the transition-metal atom subnetwork. The measured amplitudes $|F_T|$ of this partial structure factor, as a function of $Q_\perp$ [24]

$$Q_\perp = \frac{2\pi}{a}\left(\frac{\tau(N\tau - M)}{2(2+\tau)}\right)^{1/2}$$

go to zero for $Q_\perp$-values of about $0.7 \times 2\pi/a$ (where $a = 6.497$ Å is still the lattice parameter of the 6D cubic lattice). The $A_{3\perp}$ acceptance function can be any hypersurface in $R_{3\perp}$ but has to be invariant under the 120 operations of the $m\bar{3}\bar{5}$ point-group symmetry. In particular, $m\bar{3}\bar{5}$ has a centre of inversion which imposes $G_T(\boldsymbol{Q}_\perp)$, the FT of the acceptance functions $A_{3\perp}$, to be positive or negative real numbers. Additionally, $\delta_T(\boldsymbol{Q}_6)$ is the structure factor of a 6D primitive cubic lattice and, as such, is also a real number. Finally, $F_T(\boldsymbol{Q}_\parallel)$, as the product $\delta_T(\boldsymbol{Q}_6)\cdot G_T(\boldsymbol{Q}_\perp)$, is also a real number to which it is

reasonable to assign positive and negative values respectively when $Q_\perp$ is smaller and larger than $0.7 \times 2\pi/a$ (within the measured range of $Q_\perp$-values). Now, phases of the $F_{Al}(\boldsymbol{Q}_\parallel)$ partial structure factors can also be very easily reconstructed since diffraction data give phase differences between F_T and F_{Al} equal to 0 or π only. The resulting $F_{Al}(Q_\perp)$ and $F_T(Q_\perp)$ with their 'reconstructed' phases are represented in figure 2 and compared to $G(Q_\perp)$ functions corresponding to spherical acceptance functions. The numerical values and (N, M) indexing are also gathered in table 1. They can now be used straightforwardly to derive the structure. The spherical approximation for $A_{3\perp}$, actually, will not be used in this derivation and the representation shown in figure 2 is just for the sake of illustration and to support the idea that $F_T(Q_\perp)$ turns from positive to negative values when passing through zero at $Q_\perp = 0.7 \times 2\pi/a$.

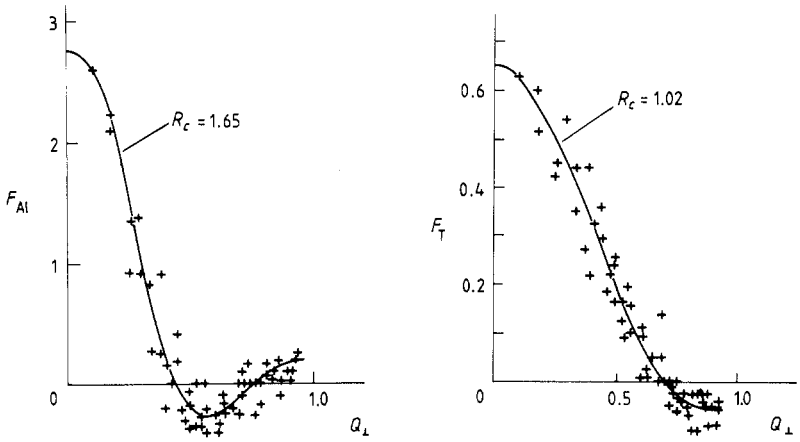

Figure 2. $Q_\perp$-dependences of the Al and Mn partial structure factors of the quasi-crystalline structure: crosses, data; full curve, best fits in the sphere approximation. Phases have been 'reconstructed' as explained in the text. Radii R_c of the spherical acceptance functions are given. They are to be compared to the radius $1.013a$ of a sphere that would have the same volume as the triacontahedron obtained by projection into $R_{3\perp}$ of the 6D cubic elementary cell. R_c(Al) and R_c(TM) are in a ratio roughly equal to τ.

3. The structure of the $Al_{74}Si_5Mn_{21}$ quasi-crystal

The first obvious procedure to generate the real atomic structure is to Fourier-transform the structure factors according to

$$\rho_T(\boldsymbol{r}) = \sum_{\boldsymbol{Q}_\parallel} F_T(\boldsymbol{Q}_\parallel) \exp(i\boldsymbol{Q}_\parallel \cdot \boldsymbol{r}) \qquad \rho_{Al}(\boldsymbol{r}) = \sum_{\boldsymbol{Q}_\parallel} F_{Al}(\boldsymbol{Q}_\parallel) \exp(i\boldsymbol{Q}_\parallel \cdot \boldsymbol{r}) \tag{7}$$

in which ρ_T and ρ_{Al} are the partial 3D atomic densities at $\boldsymbol{r}$. In particular, the average partial densities should be given by

$$\bar{\rho}_T = \sum_r \rho_T(\boldsymbol{r}) = F_T(\boldsymbol{Q}_\parallel = 0) \qquad \bar{\rho}_{Al} = F_{Al}(\boldsymbol{Q}_\parallel = 0).$$

As

$$Q_\parallel = \frac{2\pi}{a}\left(\frac{N + \tau M}{2(2+\tau)}\right)^{1/2}$$

can be equal to zero only with $N = M = 0$, F_T and F_{Al} for $Q_{\parallel} = 0$ are also given by the extrapolations of $F_T(Q_\perp)$ and $F_{Al}(Q_\perp)$ to $Q_\perp = 0$, which according to data shown in figure 2 and table 1 gives

$$F_{Al}(0)/F_T(0) = \bar{\rho}_{Al}/\bar{\rho}_T = 4.23.$$

Thus the ideal composition of the icosahedral phase would be $Al_{4.23}Mn$ or $Al_{80.9}Mn_{19.1}$. The nominal composition of the measured system being $Al_{74}Si_5Mn_{21}$, this implies that atomic sites may be occupied by different chemical species and/or that the structure could be defective. It could be due also to changes in the composition as a result of the quenching procedure. Atomic coordinates, occupation fractions within each subnetwork and distances from the origin are given in tables 2 and 3 for a few of the many calculated atomic positions. Atomic density maps representing 2D cuts of $\rho_T(r)$ and $\rho_{Al}(r)$ are also shown in figure 3. A careful examination of these results allows interesting conclusions to be drawn regarding the atomic structure. The manganese atoms are obviously at or

Table 1. Partial structure factors for Al and Mn subnetworks of an Al–Mn quasi-crystal deduced from neutron diffraction data with contrast variation. Phases have been 'reconstructed' as explained in the text.

N	M	$Q_\perp(2\pi/a)$	F_{Al}	F_T	N	M	$Q_\perp(2\pi/a)$	F_{Al}	F_T
2	1	0.707	+0.106	0	64	100	0.892	+0.050	−0.050
4	4	0.743	0	−0.020	66	105	0.632	−0.050	+0.025
6	9	0.397	−0.209	+0.422	68	108	0.673	−0.100	0
8	12	0.461	−0.220	+0.289	70	113	0.242	+0.928	+0.424
10	13	0.843	+0.071	−0.103	72	116	0.334	+0.850	+0.350
12	16	0.874	+0.107	−0.053	74	117	0.781	0	−0.025
14	21	0.610	−0.402	+0.148	76	120	0.814	+0.060	−0.025
16	24	0.650	−0.360	+0.116	78	125	0.520	−0.355	+0.187
18	29	0.167	+2.134	+0.629	80	128	0.529	−0.353	+0.095
20	32	0.282	+1.390	+0.542	82	129	0.907	+0.100	−0.050
22	33	0.762	+0.020	−0.030	84	132	0.937	+0.198	−0.061
24	36	0.795	−0.183	−0.050	86	137	0.695	−0.262	+0.141
26	41	0.490	−0.180	+0.165	88	140	0.732	+0.189	−0.051
28	44	0.539	−0.276	+0.195	90	145	0.372	+0.248	+0.325
30	45	0.888	+0.121	−0.091	92	148	0.439	+0.192	+0.292
32	48	0.918	+0.137	−0.089	94	149	0.831	+0.040	−0.025
34	53	0.699	−0.353	+0.059	96	152	0.863	+0.040	−0.025
36	56	0.710	−0.080	0	98	157	0.591	−0.375	+0.239
38	61	0.331	+0.267	+0.444	100	160	0.634	−0.160	+0.010
40	64	0.401	+0.160	+0.325	102	165	0.093	+2.620	+0.631
42	65	0.814	+0.183	−0.077	104	168	0.253	+1.350	+0.450
44	68	0.844	−0.143	−0.095	106	169	0.747	0	0
46	73	0.565	−0.416	+0.154	108	172	0.780	+0.059	−0.053
48	76	0.610	−0.340	+0.014	110	177	0.468	−0.318	+0.221
50	77	0.933	+0.138	−0.042	112	180	0.520	0	+0.125
52	84	0.175	+2.243	+0.518	114	181	0.877	0	−0.025
54	85	0.729	−0.040	−0.010	116	184	0.908	+0.040	−0.050
56	88	0.762	−0.265	−0.061	118	189	0.656	−0.213	+0.053
58	93	0.435	+0.429	+0.361	120	192	0.695	0	0
60	96	0.491	−0.066	+0.262	122	196	0.559	−0.200	+0.100
62	97	0.862	+0.200	−0.040	124	200	0.375	+0.916	+0.044

Table 2. Atomic coordinates (X, Y, Z), relative occupation fraction ρ and distance from the origin r for sites of the transition metal obtained from direct Fourier transform of the partial structure factor F_T (more distant sites are available but not given here for brevity). All distances and coordinates are given in angstroms.

Coordinates					Coordinates					Coordinates					Coordinates				
X	Y	Z	ρ	r	X	Y	Z	ρ	r	X	Y	Z	ρ	r	X	Y	Z	ρ	r
0.00	0.00	0.00	1.00	0.00	6.33	8.77	2.38	0.26	11.08	12.64	10.23	3.90	0.83	16.72	12.66	7.81	12.64	0.34	19.52
0.00	2.43	3.92	0.73	4.61	8.77	2.38	6.33	0.26	11.08	2.41	16.55	0.00	0.83	16.73	7.81	12.64	12.66	0.34	19.52
2.43	3.92	0.00	0.73	4.61	2.38	6.33	8.77	0.26	11.08	16.55	0.00	2.41	0.83	16.73	10.24	14.14	8.72	0.34	19.52
3.92	0.00	2.43	0.73	4.61	0.00	12.59	0.00	0.92	12.59	0.00	2.41	16.55	0.83	16.73	14.14	8.72	10.24	0.34	19.52
0.00	0.00	7.69	0.63	7.69	12.59	0.00	0.00	0.92	12.59	6.33	6.33	14.14	0.83	16.73	8.72	10.24	14.14	0.34	19.52
0.00	7.69	0.00	0.63	7.69	0.00	0.00	12.59	0.92	12.59	6.33	14.14	6.33	0.83	16.73	6.33	16.55	10.23	0.99	20.46
7.69	0.00	0.00	0.63	7.69	3.92	10.23	6.33	0.94	12.65	14.14	6.33	6.33	0.83	16.73	16.55	10.23	6.33	0.99	20.46
2.41	6.33	3.90	0.68	7.81	10.23	6.33	3.92	0.94	12.65	6.31	16.55	2.41	0.79	17.88	10.23	6.33	16.55	0.99	20.46
6.33	3.90	2.41	0.68	7.81	6.33	3.92	10.23	0.94	12.65	16.55	2.41	6.31	0.79	17.88	14.14	14.14	6.33	0.66	20.98
3.90	2.41	6.33	0.68	7.81	10.23	8.74	0.00	0.55	13.45	2.41	6.31	16.55	0.79	17.88	14.14	6.33	14.14	0.66	20.98
6.29	6.33	1.47	0.29	9.04	8.74	0.00	10.23	0.55	13.45	3.92	10.23	14.14	0.79	17.89	6.33	14.14	14.14	0.66	20.98
6.33	1.47	6.29	0.29	9.04	0.00	10.23	8.74	0.55	13.45	14.14	3.92	10.23	0.79	17.89	10.24	16.55	7.81	0.66	20.98
1.47	6.29	6.33	0.29	9.04	7.81	10.24	3.90	0.55	13.46	10.23	14.14	3.92	0.79	17.89	16.55	7.81	10.24	0.66	20.98
3.92	7.80	2.39	0.29	9.05	10.24	3.90	7.81	0.55	13.46	12.66	12.64	0.00	0.79	17.89	7.81	10.24	16.55	0.66	20.98
7.30	2.39	3.92	0.29	9.05	3.90	7.81	10.24	0.55	13.46	12.64	0.00	12.66	0.79	17.89	12.66	2.41	16.55	0.66	20.98
2.39	3.92	7.80	0.29	9.05	3.92	12.66	2.41	0.55	13.47	0.00	12.66	12.64	0.79	17.89	16.55	12.66	2.41	0.66	20.98
2.43	8.72	0.00	0.29	9.05	12.66	2.41	3.92	0.55	13.47	2.38	16.55	7.80	0.39	18.45	2.41	16.55	12.66	0.66	20.98
8.72	0.00	2.43	0.29	9.05	2.41	3.92	12.66	0.55	13.47	16.55	7.80	2.38	0.39	18.45	16.55	2.43	14.16	0.62	21.92
0.00	2.43	8.72	0.29	9.05	8.74	10.24	6.33	0.50	14.88	7.80	2.38	16.55	0.39	18.45	2.43	14.16	16.55	0.62	21.92
0.00	10.23	3.92	0.96	10.95	10.24	6.33	8.74	0.50	14.88	12.62	10.23	8.76	0.39	18.45	14.16	16.55	2.43	0.62	21.92
10.23	3.92	0.00	0.96	10.95	6.33	8.74	10.24	0.50	14.88	10.23	8.76	12.62	0.39	18.45	12.66	12.66	12.66	0.61	21.92
3.92	0.00	10.23	0.96	10.95	7.83	0.00	12.66	0.50	14.88	8.76	12.62	10.23	0.39	18.45	10.24	16.55	12.66	0.92	23.22
6.33	6.33	6.33	0.96	10.96	0.00	12.66	7.83	0.40	14.88	0.00	10.23	16.55	1.00	19.46	16.55	12.66	10.24	0.92	23.22
3.95	10.23	1.47	0.26	11.06	12.66	7.83	0.00	0.50	14.88	16.55	0.00	10.23	1.00	19.46	12.66	10.24	16.55	0.92	23.22
10.23	1.47	3.95	0.26	11.06	14.16	3.92	2.41	0.50	14.89	10.23	16.55	0.00	1.00	19.46	16.55	10.23	14.14	0.89	24.05
1.47	3.95	10.23	0.26	11.06	3.92	2.41	14.16	0.50	14.89	16.55	10.23	1.49	0.34	19.51	14.14	16.55	10.23	0.89	24.05
7.80	7.87	0.00	0.26	11.07	2.41	14.16	3.92	0.50	14.89	1.49	16.55	10.23	0.34	19.51	10.23	14.14	16.55	0.89	24.05
7.87	0.00	7.80	0.26	11.07	10.23	3.90	12.64	0.83	16.72	10.23	1.49	16.55	0.34	19.51	14.14	14.14	14.14	0.48	24.49
0.00	7.80	7.87	0.26	11.07	3.90	12.64	10.23	0.83	16.72	12.64	12.66	7.81	0.34	19.52					

Table 3. Same as in table 2 but for aluminium atoms.

Coordinates					Coordinates					Coordinates					Coordinates				
X	*Y*	*Z*	ρ	*r*	*X*	*Y*	*Z*	ρ	*r*	*X*	*Y*	*Z*	ρ	*r*	*X*	*Y*	*Z*	ρ	*r*
0.00	0.00	0.00	0.30	0.00	6.33	0.00	3.92	0.47	7.44	10.23	0.96	0.00	0.48	10.27	2.41	8.74	7.83	0.90	11.98
0.00	2.39	0.93	0.31	2.57	0.00	0.00	7.67	0.59	7.67	0.96	0.00	10.23	0.48	10.27	0.00	6.33	10.23	0.54	12.03
2.39	0.93	0.00	0.31	2.57	0.00	7.67	0.00	0.59	7.67	0.00	5.40	8.74	0.37	10.27	6.33	10.23	0.00	0.54	12.03
0.93	0.00	2.39	0.31	2.57	7.67	0.00	0.00	0.59	7.67	5.40	8.74	0.00	0.37	10.27	10.23	0.00	6.33	0.54	12.03
1.49	1.49	1.49	0.31	2.57	2.41	6.33	3.92	0.66	7.82	8.74	0.00	5.40	0.37	10.27	4.81	7.83	7.81	0.45	12.06
0.00	2.41	3.90	0.61	4.58	6.33	3.92	2.41	0.66	7.82	2.39	8.76	4.82	0.48	10.28	7.83	7.81	4.81	0.45	12.06
2.41	3.90	0.00	0.61	4.58	3.92	2.41	6.33	0.66	7.82	8.76	4.82	2.39	0.48	10.28	7.81	4.81	7.83	0.45	12.06
3.90	0.00	2.41	0.61	4.58	2.41	3.92	7.81	0.91	9.07	4.82	2.39	8.76	0.48	10.28	0.94	10.23	6.33	0.45	12.06
0.00	0.00	4.79	0.92	4.79	3.92	7.81	2.41	0.91	9.07	0.00	10.23	3.92	0.36	10.95	10.23	6.33	0.94	0.45	12.06
0.00	4.79	0.00	0.92	4.79	7.81	2.41	3.92	0.91	9.07	10.23	3.92	0.00	0.36	10.95	6.33	0.94	10.23	0.45	12.06
4.79	0.00	0.00	0.92	4.79	1.49	6.33	6.33	0.91	9.07	3.92	0.00	10.23	0.36	10.95	1.49	11.73	2.39	0.45	12.06
1.35	3.92	2.43	0.82	4.80	6.33	6.33	1.49	0.91	9.07	6.33	6.33	6.33	0.36	10.96	11.73	2.39	1.49	0.45	12.06
3.92	2.43	1.35	0.82	4.80	6.33	1.49	6.33	0.91	9.07	1.49	3.90	10.23	0.91	11.04	2.39	1.49	11.73	0.45	12.06
2.43	1.35	3.92	0.82	4.80	0.00	2.43	8.74	0.91	9.07	3.90	10.23	1.49	0.91	11.04	2.43	11.15	3.92	0.45	12.07
1.50	3.92	2.43	0.93	4.85	2.43	8.74	0.00	0.91	9.07	10.23	1.49	3.90	0.91	11.04	11.15	3.92	2.43	0.45	12.07
3.92	2.43	1.50	0.93	4.85	8.74	0.00	2.43	0.91	9.07	0.00	7.81	7.81	0.91	11.05	3.92	2.43	11.15	0.45	12.07
2.43	1.50	3.92	0.93	4.85	0.00	7.80	4.84	0.73	9.18	7.81	7.81	0.00	0.91	11.05	5.40	6.31	8.76	0.45	12.07
0.00	5.38	3.90	0.72	6.65	7.80	4.84	0.00	0.73	9.18	7.81	0.00	7.81	0.91	11.05	6.31	8.76	5.40	0.45	12.07
5.38	3.90	0.00	0.72	6.65	4.84	0.00	7.80	0.73	9.18	2.41	6.33	8.74	0.91	11.06	8.76	5.40	6.31	0.45	12.07
3.90	0.00	5.38	0.72	6.65	3.90	5.40	6.33	0.73	9.19	6.33	8.74	2.41	0.91	11.06	0.00	0.00	12.57	0.38	12.57
1.49	1.49	6.31	0.72	6.65	5.40	6.33	3.90	0.73	9.19	8.74	2.41	6.33	0.91	11.06	0.00	12.57	0.00	0.38	12.57
1.49	6.31	1.49	0.72	6.65	6.33	3.90	5.40	0.73	9.19	10.23	3.90	4.84	0.90	11.97	12.57	0.00	0.00	0.38	12.57
6.31	1.49	1.49	0.72	6.65	1.50	8.74	2.41	0.73	9.19	3.90	4.84	10.23	0.90	11.97	3.92	10.23	6.33	0.39	12.65
2.41	3.90	4.82	0.72	6.66	8.74	2.41	1.50	0.73	9.19	4.84	10.23	3.90	0.90	11.97	10.23	6.33	3.92	0.39	12.65
3.90	4.82	2.41	0.72	6.66	2.41	1.50	8.74	0.73	9.19	10.23	3.90	4.84	0.90	11.97	6.33	3.92	10.23	0.39	12.65
4.82	2.41	3.90	0.72	6.66	0.00	4.84	7.81	0.64	9.19	3.90	4.84	10.23	0.90	11.97	3.90	7.81	10.23	0.77	13.45
0.00	6.33	2.41	0.34	6.77	4.84	7.81	0.00	0.64	9.19	4.84	10.23	3.90	0.90	11.97	7.81	10.23	3.90	0.77	13.45
6.33	2.41	0.00	0.34	6.77	7.81	0.00	4.84	0.64	9.19	0.00	2.43	11.73	0.90	11.98	10.23	3.90	7.81	0.77	13.45
2.41	0.00	6.33	0.34	6.77	3.93	7.80	5.40	0.48	10.27	2.43	11.73	0.00	0.90	11.98	3.90	7.81	10.23	0.77	13.45
3.92	3.92	3.92	0.34	6.78	7.80	5.40	3.93	0.48	10.27	11.73	0.00	2.43	0.90	11.98					
0.00	3.92	6.33	0.47	7.44	5.40	3.93	7.80	0.48	10.27	8.74	7.83	2.41	0.90	11.98					
3.92	6.33	0.00	0.47	7.44	0.00	10.23	0.96	0.48	10.27	7.83	2.41	8.74	0.90	11.98					

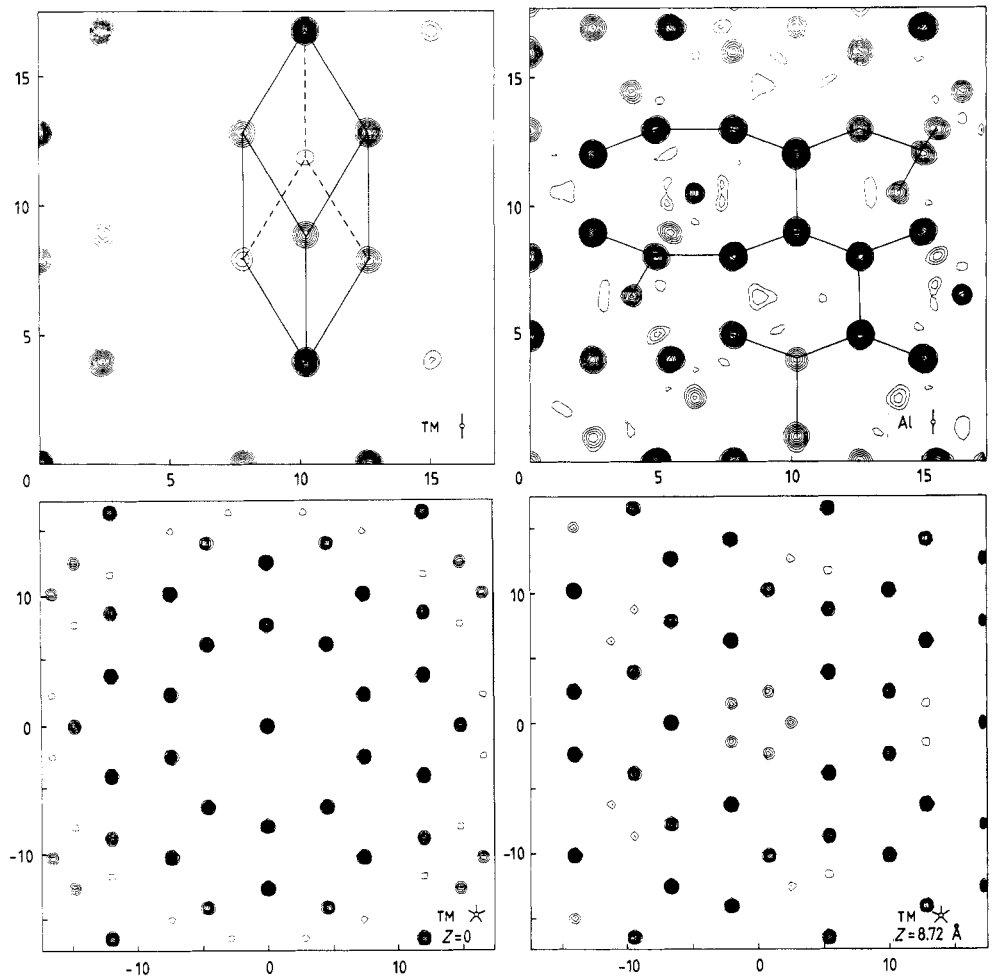

Figure 3. Samples of density maps obtained by direct Fourier transforms of the measured partial structure factors (with phases reconstructed). These maps are 2D cuts of 3D atomic density, perpendicular to 5-fold (bottom) and 2-fold (top) axes, of the 3D partial atomic densities for Al and Mn as indicated. (Level Z of the cut is given when relevant parameter for comparison.) A perspective view of one prolate rhombohedron has been drawn for the sake of illustrating the transition-metal subnetwork. Portions of chains made of antisymmetric tetrahedra are visible in the aluminium density map. All scales are in Å.

very near the vertices of a 3DPT with 4.6 Å edges. But the occupation fractions are very often smaller than 1. The two vertices at the short diagonals of the oblate rhombohedra, separated by 2.59 Å, are scarcely occupied simultaneously by Mn atoms. From the examination of table 3 (or rather a more extended one not presented here for the sake of brevity), it appears that the major Al sites are:

(i) at vertices or near vertex positions shared with Mn atoms;

(ii) near positions situated at 2.57 and 6.78 Å from the vertices on the triad axis of the prolate rhombohedra (10.96 Å for this triad axis and 13.55 Å if an oblate rhombohedron is aligned properly); and

(iii) near positions on the faces, dividing the long diagonals of the rhombi into segments of 2.98 and 4.83 Å (7.81 Å for the diagonal).

Judging from the occupancy values ρ displayed in table 3, these different Al sites apparently are never simultaneously occupied in a given rhombohedron of the 3DPT. This is fortunate for obvious steric constraints and introduces a 'chemical modulation' of the structure which may be welcome to allow stability of the whole architecture. A schematic illustration of the corresponding decoration is shown in figure 4. The weak point in this procedure of a direct FT of the partial structure factors is obviously that the structure can actually be described only with an extensive list of atom coordinates, which is not very easy to manipulate. Moreover, possible spurious truncation effects are not easily detected. Thus, it might be sensible to analyse the structure in 6D first, in order to recover the hidden translational symmetry, and then, if necessary, generate the 3D atomic decoration by projection or cut of the decorated 6D structure.

Looking back at equation (6) expressing the partial structure factors $F_{Al}(\boldsymbol{Q}_\parallel)$ and $F_T(\boldsymbol{Q}_\parallel)$ suggests that they can be considered as $\boldsymbol{Q}_6$-dependent since a well defined $\boldsymbol{Q}_6$ in the 6D reciprocal space is attached to a given $\boldsymbol{Q}_\parallel$, i.e.

$$F_{Al}(\boldsymbol{Q}_6) = \delta_{Al}(\boldsymbol{Q}_6)\cdot G_{Al}(\boldsymbol{Q}_\perp) \qquad F_T(\boldsymbol{Q}_6) = \delta_T(\boldsymbol{Q}_6)\cdot G_T(\boldsymbol{Q}_\perp).$$

When Fourier-transformed in 6D space, these functions give the partial Al and TM density distributions $\rho_{Al}(\boldsymbol{r}_6)$ and $\rho_T(\boldsymbol{r}_6)$ convoluted with the respective acceptance functions $A_{3\perp}(\text{Al})$ and $A_{3\perp}(\text{TM})$. The result is of course a 6D periodic structure whose nodes are decorated by the above acceptance functions. Thus, two basic structural ingredients can be readily derived, i.e. the *6D coordinates of the sites* and the *corresponding acceptance*

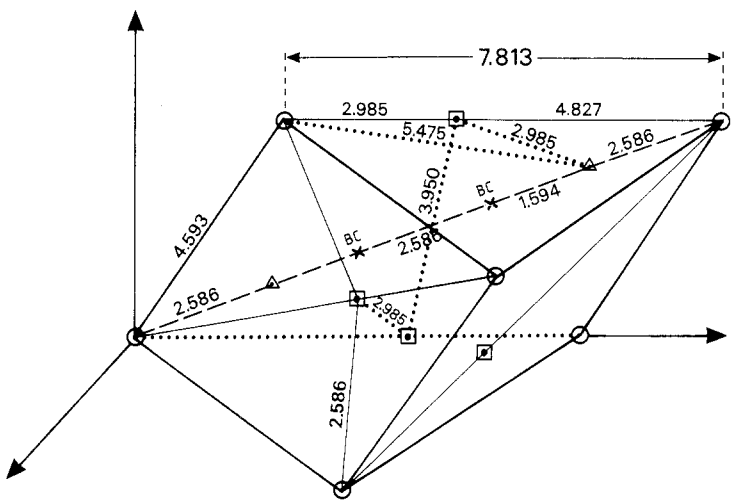

Figure 4. Schematic presentation of the atomic decoration of half a prolate rhombohedron. ○, Transition-metal site corresponding to node sites in 6D with a pseudo-spherical acceptance function. □, Al sites on the long diagonals of the faces. △, Al sites on the triad axis. (□ and △ correspond to node sites in 6D with a pseudo-spherical shell as an acceptance function.) ×, Al sites on the triad axis corresponding to the body centres in 6D with a very fuzzy spherical distribution as an acceptance function. The decoration of the oblate rhombohedra is very similar to the one represented here except for the two types of triad axis sites which do not exist any more. As explained in the text, all these sites are partially occupied only; for instance, about half of the face sites of the oblate rhombohedra are empty and so are the triad axis sites of the prolate rhombohedron.

functions for each of the atomic species. Surprisingly enough what has emerged from calculations is a very simple, CsCl-like structure, as illustrated in figure 5, which presents 2D rational cuts of the 6D space containing one axis of each of the ($R_{3\parallel}$, $R_{3\perp}$) subspaces.

There is obviously only one atomic site for the TM atoms (figure 5 TM), very well located at the vertices of the 6D cubic lattice. The $A_{3\perp}$ acceptance function can be better illustrated with a 2D cut in the $R_{3\perp}$ subspace as shown in figure 6. This acceptance function exhibits an obvious spherical symmetry, with a fairly well defined density plateau in its central part. However, the borders of the strip are not sharp and do not define an all-or-nothing straight cut in the 6D space. If the density at the plateau is normalised to unity,

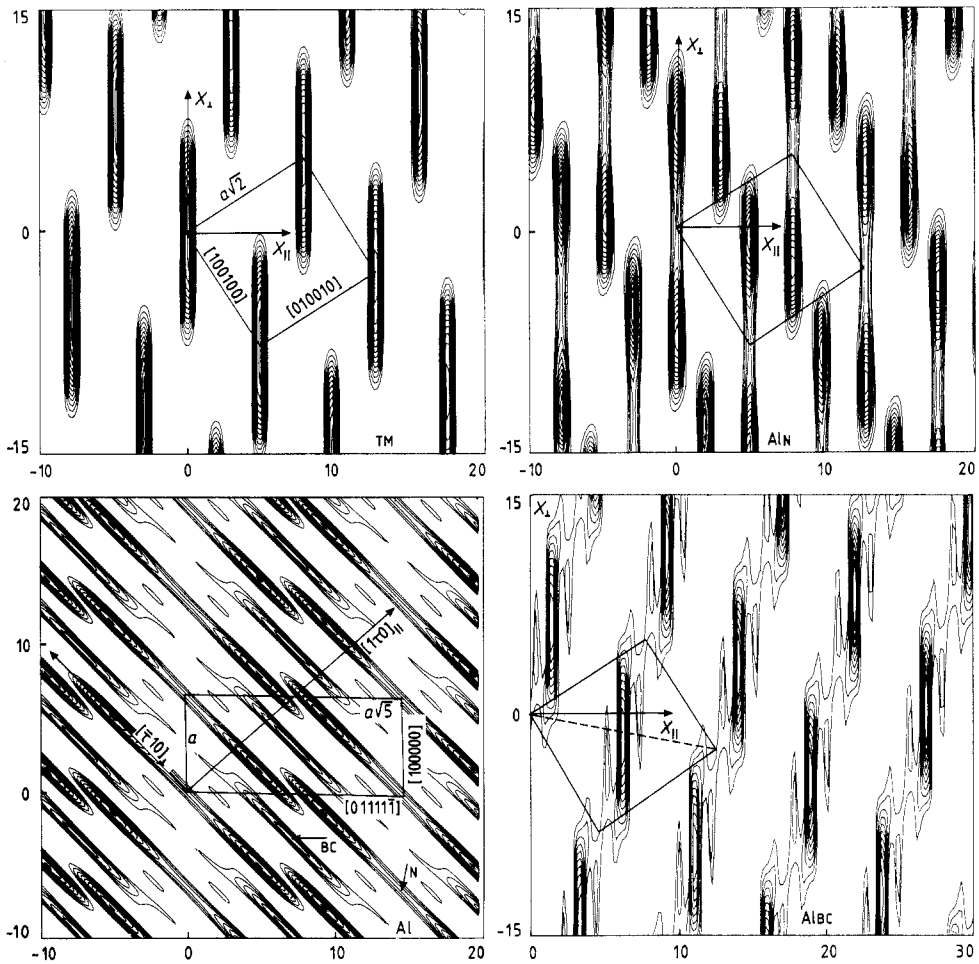

Figure 5. Samples of 2D cut of the 6D periodic partial atomic densities. The transition-metal site is unique, at the nodes of the 6D cubic lattice; its acceptance function 'decorates' the site. There are two different aluminium sites, one at the nodes and the second one at the body centres, also 'decorated' with the pertinent acceptance functions. The cut sections of the 6D cubic unit cell are shown along with the coordinate axis of the cut. TM stands for the transition-metal atom sites, AlN and AlBC for aluminium node sites and body-centre sites, respectively. The AlBC node shown here is the $(\frac{3}{2}, \frac{1}{2}, \frac{1}{2}, \frac{1}{2}, \frac{1}{2}, \frac{1}{2})$ one corresponding to $X_\parallel = 6.33$, $Y_\parallel = 7.82$, $Z_\parallel = 3.92$, $X_\perp = -1.49$, $Y_\perp = 4.82$ and $Z_\perp = 2.42$ (Å). The axes are in Å.

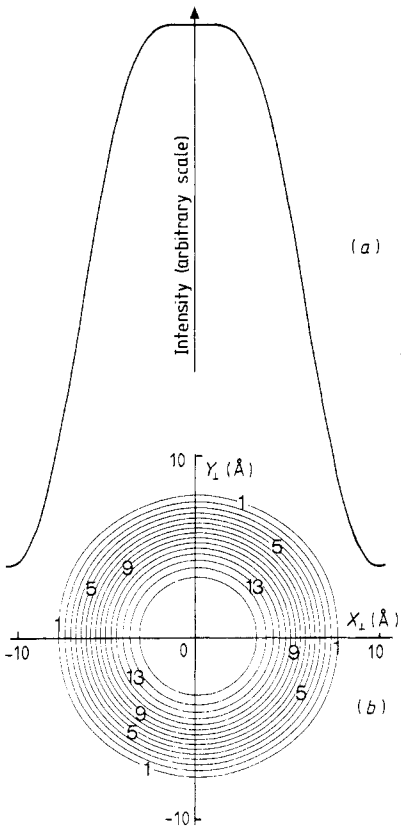

Figure 6. Radial density (*a*) and 2D projection (*b*) of the $A_{3\perp}$(TM) acceptance function in $R_{3\perp}$, showing its pseudo-spherical symmetry and the smoothing of its borders with respect to a strict spherical cutting.

the total integrated volume of $A_{3\perp}$(TM) is of the order of $0.9 \times 4\pi a^3/3$. This is about 87% of the volume of the triacontahedron that would result from the projection into $R_{3\perp}$ of the elementary 6D cubic unit cell. Within uncertainties due to truncation effects (see § 4) this 87% is also the average occupancy fraction of the projected 3DPT vertices by the manganese (or TM) atoms [27].

There are two different sites for Al atoms in 6D (figures 5 AlN and AlBC). One is located also at the 6D lattice nodes (N sites hereafter) and the other one is body-centred $(\frac{1}{2}, \frac{1}{2}, \frac{1}{2}, \frac{1}{2}, \frac{1}{2}, \frac{1}{2})$ in 6D (BC sites hereafter).

The N sites have an acceptance function $A_{3\perp}$(AlN) which can be roughly described as a spherical shell (figure 7). The inner sphere has a radius of about $1.05a$ with a density of the order of 0.35 and the outer limit a radius of about $2a$ with a maximum occupancy ratio of 81% for the projected sites. The total integrated volume of $A_{3\perp}$(AlN) is $3.2 \times 4\pi a^3/3$.

The BC sites have an acceptance function $A_{3\perp}$(AlBC) whose symmetry is still almost spherical but with a continuously decreasing density from its centre, and a total integrated volume of about $0.5 \times 4\pi a^3/3$ (figure 8). This volume is equal to 47% of the ideal triacontahedral acceptance function and gives the occupancy ratio of the Al sites in 3D that result from the projection of the 6D BC sites.

When considered altogether, the atomic decoration, deduced from the Fourier transform in 6D of the measured partial structure factors, is perfectly consistent with the results of direct calculations in 3D. It is worth pointing out that the correspondence

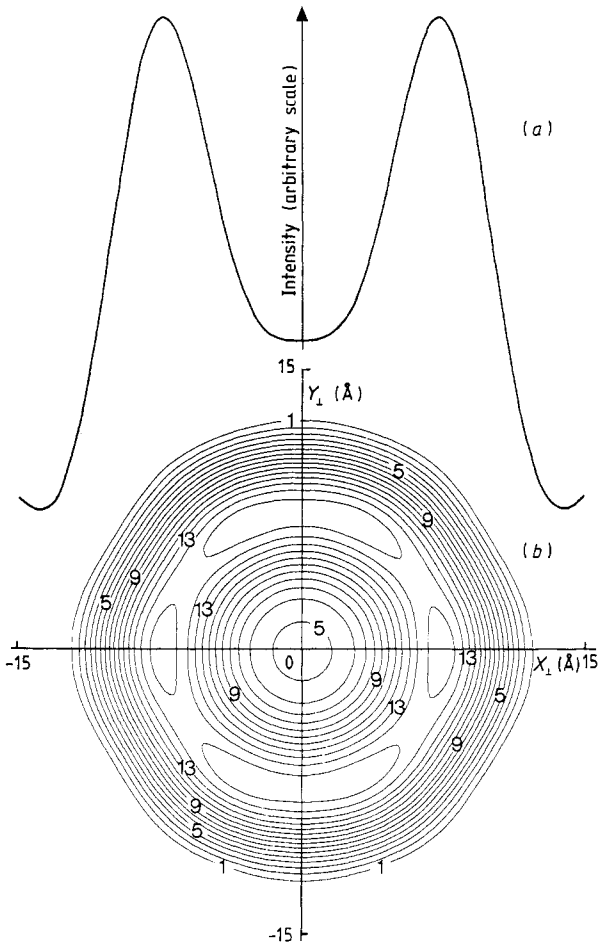

Figure 7. Same representation as in figure 6 but for the Al node sites. The $A_{3\perp}$(AlN) is clearly shell-like, with an inner almost excluded volume corresponding roughly to $A_{3\perp}$(TM). Borders show also a certain fuzziness and anisotropy.

between 6D and 3D densities is rather straightforward. As an example, the left bottom part of figure 5, showing a 2D cut of the two different sites of the Al sublattice, is very illustrative. This map contains among other things the fivefold axis $[1\tau 0]_\parallel$ of the physical space. The atomic density in 3D along this axis is readily obtained by measuring it directly in 6D, that is by collecting the intersections of the $[1\tau 0]_\parallel$ axis with the density features which show up in the map. Moreover, additional information has been gained with the determination of the volumes and shapes of the acceptance functions. The average site occupancy fractions are now fairly well known and appear as related to the topology of the strips which are cut in 6D to generate the projected 3D structure. These strips may have waving features and/or rough surfaces, or even be constituted by a distribution of unconnected small clusters around a larger volume (figure 9). Consequently, the cross section of these strips into $R_{3\perp}$ may appear as spherical or almost spherical distributions with continuously changing density rather than the 'one-inside/zero-outside' elementary scheme. Such a 'fuzziness' in the strip definition is obviously the 6D way to describe the 'chemical modulation' or occupancy modulation of the atomic sites in 3D and introduces a 'controlled disorder' that might explain diffuse scattering effects reported elsewhere [28, 29]. However, truncation effects, as explained later in this paper, may also be responsible for a part of this 'wall fuzziness'.

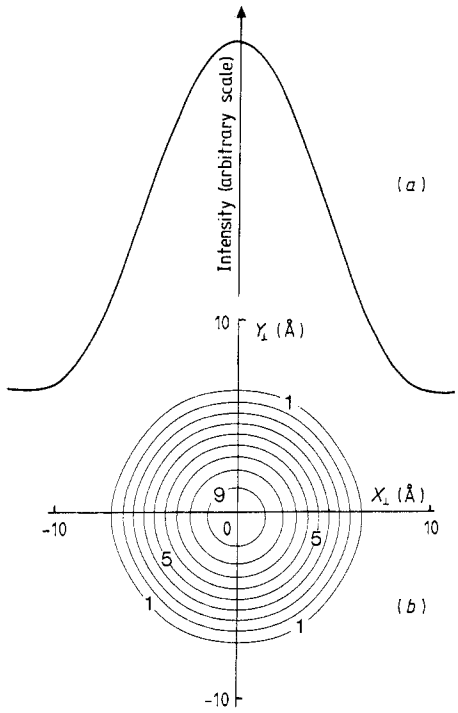

Figure 8. Same representation as in figures 6 and 7 but for the Al body-centre sites. The $Al_{3\perp}(Al_{BC})$ shows a pronounced maximum at its centre and induces a strong occupancy modulation for the corresponding sites projected into 3D.

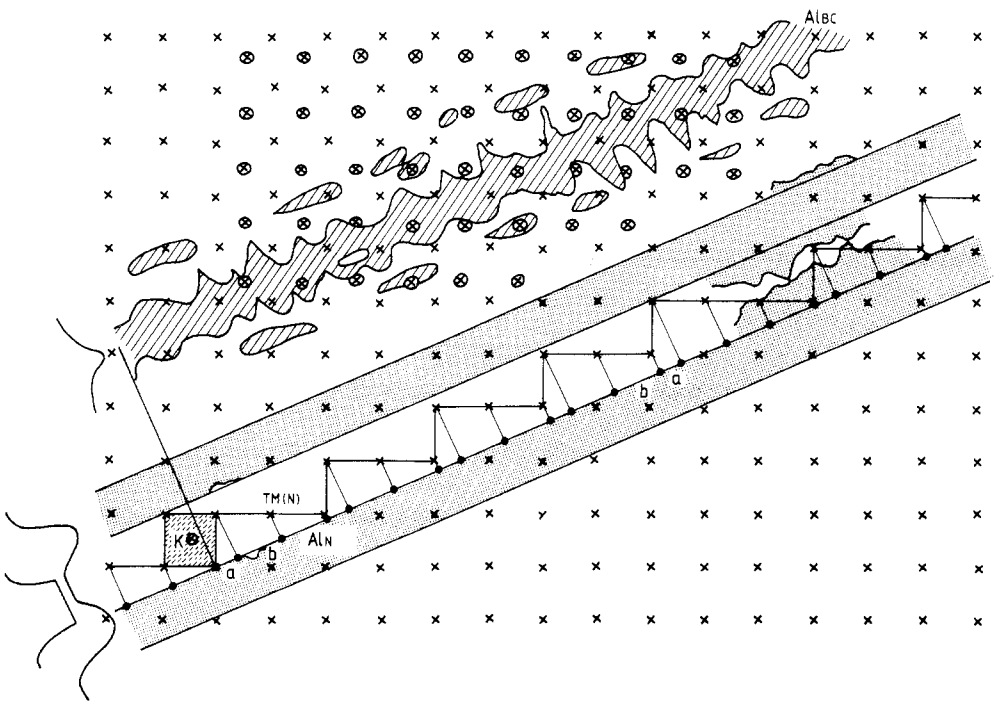

Figure 9. 2D illustration of a multiple strip generation of a 1D quasi-periodic structure. Fuzziness or roughness of the strip borders are accounted for by inclusion of 2D clusters into the acceptance functions which, in turn, generate 'chemical modulation' or 'controlled disorder' in the 1D projected structure.

The occupancy fraction of the face sites by Al atoms would correspond roughly to only half of these sites really being occupied at the faces of the *oblate* rhombohedron, which, combined with the occupancy of the triad axis sites, induce natural rules for matching the rhombic faces and forbid the existence of too short atomic distances.

The concentration of each site in the material composition is directly proportional to the volume of its acceptance function, i.e. 0.9 for the TM atoms, 3.2 for the AlN and 0.5 for the AlBC atoms. This gives a normalised formula $Al^{N}_{69.6}Al^{BC}_{10.8}TM^{N}_{19.6}$ or $Al_{80.4}TM_{19.6}$. The average density may also be evaluated by the total volume of the acceptance functions compared to the 6D unit cell; such an estimate gives $\bar{\rho} = 0.07$ at.Å^{-3} or 3.8 g cm^{-3}. Both calculated composition and density are in better than good agreement with experimental values.

It has to be stressed also that the present work quantifies for the first time the chemical and force constants disorder which was observed earlier in structural or dynamic studies of quasi-crystals [30–32].

4. Possible effects from truncation in the reciprocal space

The point to be discussed now is the consequences on the calculated density of the experimental limitation of the accessible Q-range.

In the Fourier analysis of periodic crystals, all the information on the perfect structure is contained in well defined 'strong' Bragg peaks whose intensity and number become rather weak at large $Q_{\parallel}$-values. Thus, the limitation in the accessible $Q_{\parallel}$-range (typically 8 Å^{-1}) has no drastic influence on the calculated density, beyond space resolution effects and fuzzy ripples within the background. On the other hand, $Q_{\perp}$ is not a relevant parameter for a periodic crystal.

For quasi-periodic crystals, the range limitation in $R^{*}_{3\parallel}$ has practically the same kind of acceptable effects as for periodic crystals. But there may be a much stronger influence coming from the truncation in $\boldsymbol{Q}_{\perp}$. The diffraction pattern of a quasi-crystal (in 3D) is a pseudo-continuum of Bragg peaks and only the strong ones with relatively *small* $|\boldsymbol{Q}_{\perp}|$*-values* are actually measured. For instance, in the present study, the investigated Q-range corresponds to $Q_{\parallel} \leqslant 8$ and $Q_{\perp} \leqslant 1$ (in $2\pi/a$ units) and contains in principle 283 independent diffraction peaks (8964 if multiplicities are taken into account), among which only 60 are actually measured. Had this Q-range been extended to $Q_{\perp} \simeq 3$, 5951 independent diffraction peaks (241714 with multiplicities!) would have been included.

To illustrate the point, let the hypersurface $A_{3\perp}$ be simply a sphere of radius equal to a in the 3D $R_{3\perp}$ complementary space, decorating the nodes of a 6D primitive cubic lattice of parameter also equal to a. The $g(\boldsymbol{Q}_{\perp})$ function (FT of the $A_{3\perp}$) has a spherical symmetry with an oscillatory profile as a function of $|\boldsymbol{Q}_{\perp}|$ as shown in figure 10. If the very large $Q_{\perp}$-values, corresponding to very weak diffraction peaks actually smeared out into a background, were effectively measured, the FT of the experimental $g(Q_{\perp})$ would of course restore the sphere $A_{3\perp}$ with a one-inside/zero-outside density profile as shown (broken line) in figure 11. Unfortunately, data are restricted to values of $|\boldsymbol{Q}_{\perp}|$ typically smaller than $2\pi/a$. The corresponding FT profile is also shown in figure 11 (full curve). Thus, the truncation effects in $R_{3\perp}$ produce the expected ripples up to quite large $r_{\perp}$-values but there is also an artificial 'smoothing' of the sphere wall, with a reduction of the profile density for $0.5a < r_{\perp} < 1a$ and a significant density outside the hard original sphere to compensate; a sort of density depression is also

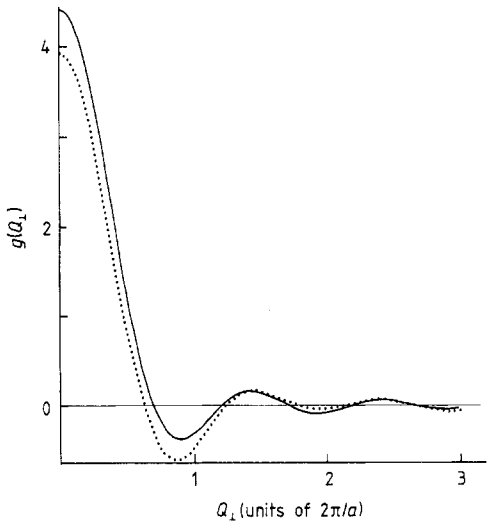

Figure 10. Fourier transform of a spherical $A_{3\perp}$ hypersurface (full curve) and of a spherical shell with the inner radius half the outer one (dotted curve).

created for $r_\perp < 0.5a$. It is easy to realise that reduction of the $A_{3\perp}$ density profile with respect to the sphere reduces the number of atoms in the cut density into $R_{3\parallel}$ while increases or extension of this profile generate additional atoms. Of course, there is no rigorous way, in practice, to determine the contribution to the observed smoothness of the wall and depression of the plateau, which are really due to truncation effects. But clearly, spurious atomic positions in 3D may come from these effects and one can get rid of them by reshaping the $A_{3\perp}$ functions issued from the FT in 6D of the diffraction data.

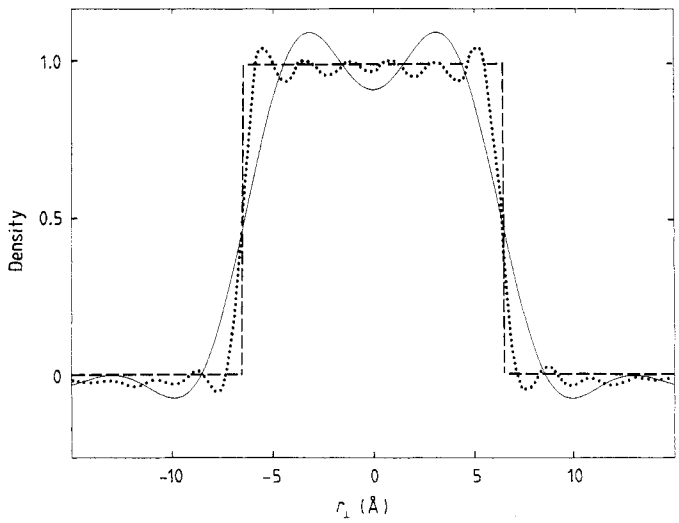

Figure 11. Illustration of the $Q_\perp$ truncation effects. The density profile in $R_{3\perp}$ of a spherical $A_{3\perp}$ function (broken line) is compared to profiles calculated by Fourier transforms of the $g(Q_\perp)$ function shown in figure 10 when cut at $Q_\perp = 1 \times 2\pi/a$ (full curve) and $Q_\perp = 3 \times 2\pi/a$ (dotted curve). Ripples, depressions and smoothing are observed, which may generate spurious atomic positions in the 3D physical space.

Incidentally it is also interesting to realise that too crude diffraction data cannot give all the answers as far as the hypersurface $A_{3\perp}$ is concerned. The point is illustrated in figure 10 where two $g(Q_\perp)$ functions are shown: one corresponds to the sphere as explained above; the other to the same sphere but with an inner centred hole of radius $0.5a$. Clearly the difference between the two will range within typical experimental accuracy. It is thus doubtful that 6D models, with decoration of the different 6D sites by a thick spherical shell, would be completely derivable from a single set of diffraction data, without contrast variation measurements. Although not illustrated in this paper, it is easy to show that truncation effects are even more drastic on a spherical shell than on a sphere, with in particular the appearance of significant density in the normally empty central hole of the shell.

5. Discussion and conclusions

Using either a direct Fourier transform in 3D of partial structure factors, with their phases reconstructed, or a description of the structure in 6D prior to projection, we have been able to derive the atomic decoration with the correct density and composition corresponding to a $Al_{74}Si_5Mn_{21}$ quasi-crystal. Obviously this decoration, deduced rather directly from neutron diffraction data, differs quite deeply from the usually accepted scheme. The Mackay icosahedron no longer appears as the basic structural unit and some atomic arrangements are introduced which cannot be found in related crystalline compounds.

The transition-metal atoms seem to form a well ordered subset with only one type of site well represented by the vertices of a 3DPT with edge length equal to about 4.6 Å. The aluminium atoms are distributed in space with more fuzziness in their site specification. They are located roughly within four categories: some vertices; points at about 2.6 and 6.8 Å from vertices on the triad axis of the prolate rhombohedra; points dividing the long diagonals of faces of both prolate and oblate rhombohedra into segments of about 3 and 4.8 Å. In a given rhombohedron all these sites are never occupied simultaneously and actual positions are somewhat scattered around the average theoretical sites. Matching rules for the oblate and prolate rhombohedra are related to occupancy of the face and triad axis sites. There is no significant evidence for mid-edge sites for Al atoms.

Such a description is in fact not at all surprising. A rigid tiling model, with all the tiles decorated with strictly equivalent sites, cannot actually be accepted. Such a scheme would result in unstable structures due to the existence of incompatible bond angles and pair distances. The transition-metal substructure propagates the long-range ordering of the whole structure while the aluminium atoms introduce the necessary 'chemical modulation' allowing stability as pointed out by Janssen [33]. The last question which might be raised concerns the positions of the silicon atoms and their obvious influence on the stability of the quasi-crystals with respect to relative crystals. A sensible assumption would be to locate these silicon atoms in the body-centred sites, on the grounds that these positions correspond to quite a small volume and may accommodate smaller atoms more easily [34]. However, the point has to be experimentally confirmed.

Finally it is probably worth pointing out that the structure described in the present work is not a 'model': the atomic positions have been *deduced* from diffraction data without any of the crystal-chemistry assumptions that are usually used to build

'reasonable' structures. As such, the paper provides the first existing list of atom coordinates, even if several sources of inaccuracy have not been completely ruled out, such as, in particular, the real extent of spurious effects due to truncation in the $Q_\perp$ reciprocal space.

A by-product of the present work might be the extension of the strip-projection method to generate 'controlled disorder', up to any wanted degree, by choosing appropriate 'strips', with rough surfaces, or including unconnected clusters in 6D, or with waving shape . . . , etc. The point was already investigated in some detail by Divincenzo [35] to describe imperfect icosahedral solids but amorphous structures might gain something if such approaches were to be used.

References

[1] Duneau M and Katz A 1985 *Phys. Rev. Lett.* **54** 2688
[2] Elser V 1985 *Phys. Rev.* B **32** 4892
[3] Elser V and Henley C L 1985 *Phys. Rev. Lett.* **55** 2883
[4] Elser V 1986 *Acta Crystallogr.* **42A** 36
[5] Zia R K P and Dallas W J 1985 *J. Phys. A: Math. Gen.* **18** L341
[6] Kalugin P A, Pitayev A Y and Levitov L S 1985 *Sov. Phys.–JETP Lett.* **41** 119
[7] Baer S 1987 *J. Phys. C: Solid State Phys.* **20** 1589
[8] Penrose R 1974 *J. Inst. Math. Appl.* **10** 266
[9] Guyot P and Audier M 1985 *Phil. Mag.* B **52** L15
[10] Henley C L and Elser V 1986 *Phil. Mag.* B **53** L59
[11] Fruchart R and Dubois J M 1987 *C. R. Acad. Sci., Paris* **305** 661, 1413
[12] Dubois J M and Janot Ch 1987 *J. Physique* **48** 1981
[13] Dubois J M, Janot Ch and Pannetier J 1986 *Phys. Lett.* **115** A177
[14] Janot Ch, Pannetier J, de Boissieu M and Dubois J M 1987 *Eur. Phys. Lett.* **3** 995
[15] Janot Ch, Dubois J M and Pannetier J 1987 *Physica* B **146** 351
[16] Janot C, Dubois J M, Pannetier J, de Boissieu M and Fruchart R 1988 *Quasicrystalline Materials* (ILL/CODEST Workshop) ed. C Janot and J M Dubois (Singapore: World Scientific) p 107
[17] Shechtman D, Blech I, Gratias D and Cahn J W 1984 *Phys. Rev. Lett.* **53** 1951
[18] Janot Ch, Pannetier J, Dubois J M and Fruchart R 1986 *Phys. Lett.* A **119** 309
[19] Janot Ch, Dubois J M and Pannetier J 1988 *Proc. Int. Workshop Quasicrystals (Beijing)* ed. K H Kuo (Aldermannsdorf, Switzerland: Trans. Tech.) p 329
[20] Shechtman D 1988 *Quasicrystalline Materials* (ILL/CODEST Workshop) ed. C Janot and J M Dubois (Singapore: World Scientific) p 3
[21] Dubois J M and Janot Ch 1988 *Eur. Phys. Lett.* **5** 235
[22] Hewat A W 1981 *ILL Report* 81HE51T
[23] Antoniadis A, Berruyer J and Filhol A 1986 *ILL Report* 86AN02T
[24] Cahn J W, Shechtman D and Gratias D 1986 *J. Mater. Res.* **1** 13
[25] Roth M, Lewit-Bentley A and Bentley G A 1984 *J. Appl. Crystallogr.* **17** 77
[26] Gratias D 1988 *Quasicrystalline Materials* (ILL/CODEST Workshop) ed. C Janot and J M Dubois (Singapore: World Scientific) p 83; 1988 *J. Physique* **49** 1225
[27] Conway J H and Knowles K M 1986 *J. Phys. A: Math. Gen.* **19** 3645
[28] Marmeggi J C, Janot C and Dubois J M 1988 *Quasicrystalline Materials* (ILL/CODEST Workshop) ed. C Janot and J M Dubois (Singapore: World Scientific) p 126
[29] Denoyer F, Heger G, Lambert M, Lang J M and Sainfort P 1987 *J. Physique* **48** 1357
[30] Knowles K M and Stobbs W M 1986 *Nature* **323** 313
[31] Betscher H, Grütter P, Indlehofer G, Jenny H, Lapka R, Oelhafen P, Wiesendanger R, Zingg T and Güntherodt H J 1987 *Z. Phys.* B **68** 313
[32] Suck J B, Bretscher H, Rudin H, Grütter P and Güntherodt H J 1987 *Phys. Rev. Lett.* **59** 102
[33] Janssen T 1986 *Acta Crystallogr.* A **42** 261
[34] Dubois J M, Janot Ch and de Boissieu M 1988 *Quasicrystalline Materials* (ILL/CODEST Workshop) ed. C Janot and J M Dubois (Singapore: World Scientific) p 97
[35] Divincenzo D P 1986 *J. Physique Coll.* **47** C3 237